Electronic Supporting Information for:

An Experimental and Master-Equation Modeling Study for the Kinetics of the Reaction between Resonance-Stabilized $(CH_3)_2CCHCH_2$ Radical and Molecular Oxygen

Satya P. Joshi, Timo T. Pekkanen, Prasenjit Seal, Raimo S. Timonen, Arkke J. Eskola[*]

Molecular Science, Department of Chemistry, University of Helsinki, P.O. Box 55(A.I. Virtasen aukio 1), FIN-00014, Helsinki, Finland

[*]*corresponding author:* arkke.eskola@helsinki.fi

Table of content

Table S1 . . . . . **S3**

Figure S1 . . . . . **S4 – S5**

Figure S2 . . . . . **S6**

Table S2 . . . . . **S7 – S9**

Table S3 . . . . . **S10 – S11**

Table S1. The experimental conditions and bi-exponential fitting parameters for intermediate temperature range measurements of reaction (1a, -1a).[a] Statistical uncertainties shown are 1σ.

T (K)	P_{He} (Torr)	λ_1 (s^{-1})	λ_2 (s^{-1})	*B*	*C*	*D*
325	0.86	174.4 ± 2.9	15.2 ± 1.3	78.7	1553.1 ± 12.9	163.0 ± 9.4
325	0.86	246.1 ± 4.1	17.8 ± 1.6	60.9	1105.3 ± 10.4	82.8 ± 5.2
330	0.88	267.8 ± 7.2	18.4 ± 1.8	193.1	1075.3 ± 18.3	104.5 ± 7.2
335	0.90	192.6 ± 3.6	11.8 ± 0.9	80.6	1305.6 ± 11.9	203.1 ± 8.2
337	0.90	218.2 ± 6.0	15.3 ± 1.0	200.3	1167.2 ± 16.8	231.9 ± 9.8
338	0.91	225.3 ± 5.6	17.2 ± 1.2	267.4	1877.1 ± 23.4	333.9 ± 15.2
344	0.92	221.1 ± 5.8	17.2 ± 0.6	186.9	1387.0 ± 18.7	452.0 ± 11.5
348	0.94	211.4 ± 6.2	16.0 ± 0.6	229.4	1479.8 ± 21.6	612.1 ± 14.1
353	0.96	190.5 ± 21.2	17.4 ± 1.6	248.0	575.6 ± 30.8	352.2 ± 23.9
356	0.96	228.0 ± 12.1	16.4 ± 0.4	278.1	1025.6 ± 29.5	947.1 ± 15.9
356[b]	1.22	224.6 ± 98.7	8.5 ± 1.3	39.1	61.0 ± 15.3	52.2 ± 3.3
358	0.97	269.6 ± 57.9	14.9 ± 1.6	598.8	466.6 ± 58.2	395.5 ± 24.5
361	0.48	182.8 ± 11.1	16.6 ± 0.5	170.9	659.6 ± 19.6	663.2 ± 14.4
361	0.96	292.1 ± 15.4	15.1 ± 0.4	162.8	601.8 ± 19.2	500.7 ± 7.3
361[b]	1.22	208.7 ± 83.5	9.1 ± 1.1	25.4	39.7 ± 9.6	53.8 ± 3.1
361[c]	3.61	217.5 ± 60.6	23.5 ± 2.2	26.9	38.6 ± 5.2	53.8 ± 4.4
361[c]	5.58	251.6 ± 86.3	26.2 ± 2.1	29.3	35.8 ± 6.1	60.8 ± 4.4
362	0.97	287.2 ± 23.3	16.3 ± 0.3	324.8	958.3 ± 56.7	1357.3 ± 15.7
367	0.71	299.0 ± 40.8	15.7 ± 0.4	262.7	567.8 ± 58.7	867.3 ± 14.7
373	0.76	383.6 ± 67.3	15.5 ± 0.3	458.6	760.7 ± 126.8	2050.7 ± 18.5
373	1.21	414.2 ± 71.4	14.8 ± 0.3	446.5	684.3 ± 100.8	1773.2 ± 16.6

[a] Xe-lamp with a sapphire window was used for detection, Pyrex-glass reactor (id = 1.65 cm) with polydimethylsiloxane (PDMS) coating, unless otherwise stated. [b] 1-chloro-3-methyl-2-butene precursor was used for the production of $(CH_3)_2CCHCH_2$ radical, pyrex-glass reactor (id = 1.65 cm) with halocarbon wax coating. [c] Stainless steel reactor (id = 0.8 cm) with halocarbon wax coating.

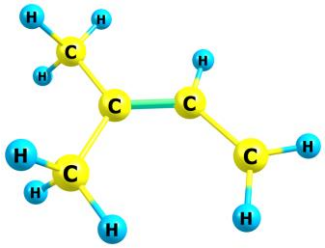

(R, $\Delta H_{(298K)}$ = 0 kcal mol^{-1})

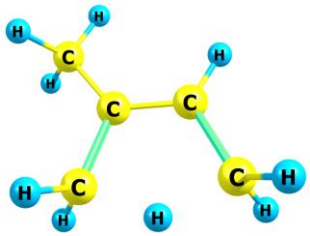

(TS1, $\Delta H_{(298K)}$ = 38.89)

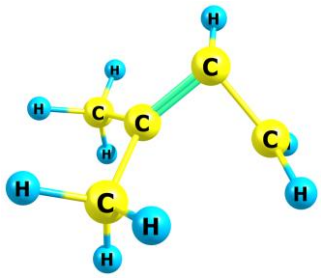

(TS2, $\Delta H_{(298K)}$ = 53.08)

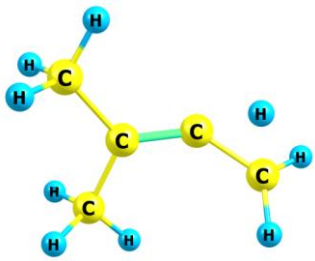

(TS3, $\Delta H_{(298K)}$ = 63.98)

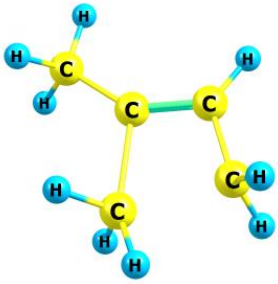

(TS4, $\Delta H_{(298K)}$ = 88.47)

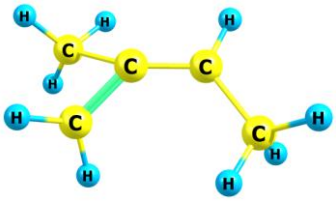

(TS5, $\Delta H_{(298K)}$ = 81.02)

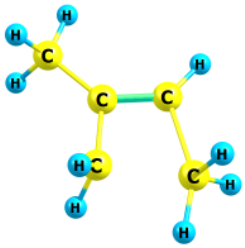

(TS6, $\Delta H_{(298K)}$ = 90.79)

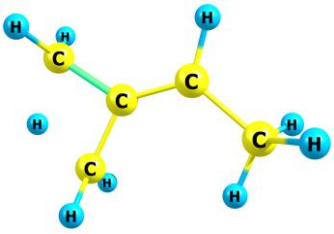

(TS7, $\Delta H_{(298K)}$ = 57.24)

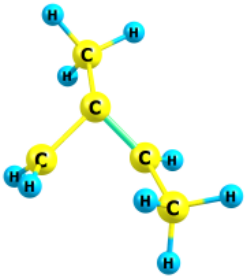

(TS8, $\Delta H_{(298K)}$ = 53.54)

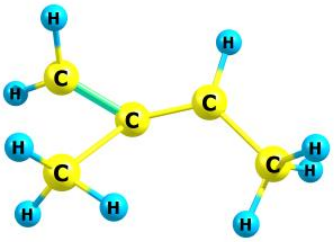

(TS9, $\Delta H_{(298K)}$ = 80.24)

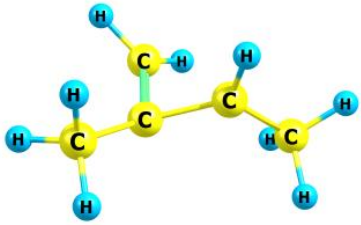

(TS10, $\Delta H_{(298K)}$ = 50.64)

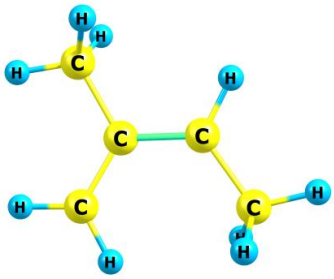

(I1, $\Delta H_{(298K)}$ = 2.10)

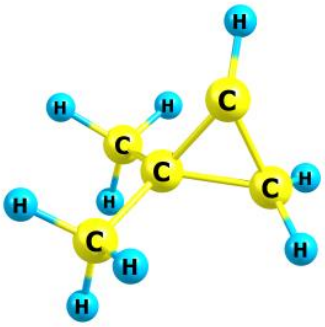

(I2, $\Delta H_{(298K)}$ = 28.25)

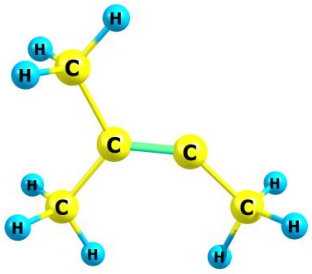

(I3, $\Delta H_{(298K)}$ = 22.86)

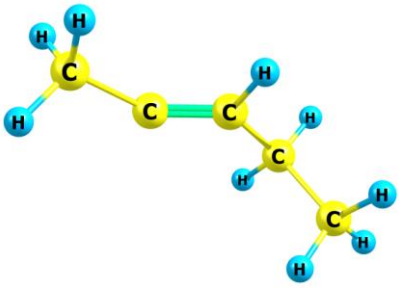

(I4, $\Delta H_{(298K)}$ = 25.61)

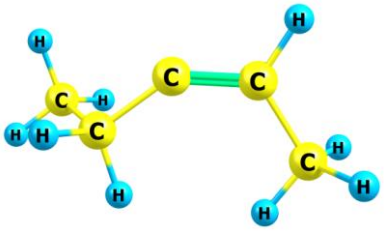

(I5, $\Delta H_{(298K)}$ = 26.56)

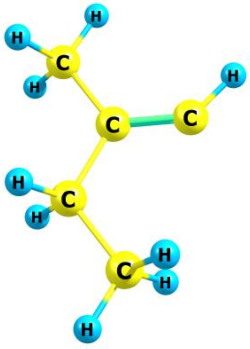

(I6, $\Delta H_{(298K)}$ = 28.28)

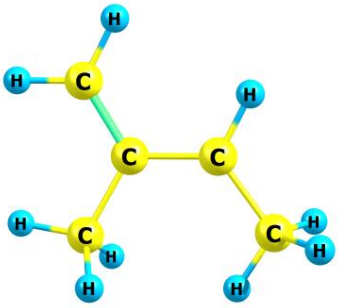

(I7, $\Delta H_{(298K)}$ = 1.83)

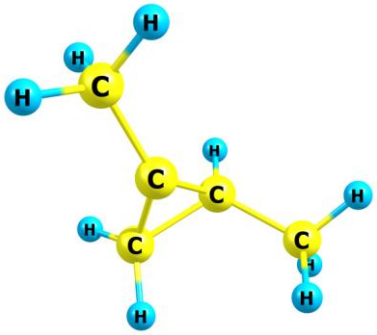

(I8, $\Delta H_{(298K)}$ = 26.28)

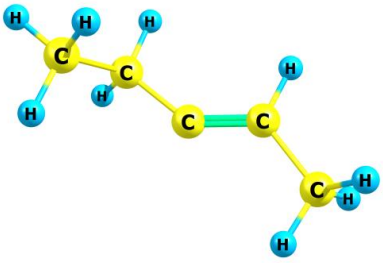

(I9, $\Delta H_{(298K)}$ = 25.94)

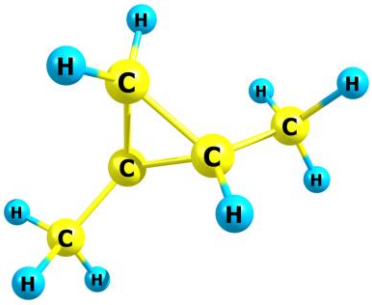

(I10, $\Delta H_{(298K)}$ = 26.28)

Figure S1. MN15/cc-pVTZ optimized geometries and $\Delta H_{(298K)}$ (kcal mol^{-1}**)** values of the stationarity points associated with $(CH_3)_2CCHCH_2$ radical isomerization.

Experimental uncertainty in the high-temperature range measurements

The Figure S2 below shows the bimolecular plot of reaction (1b) measured at T = 501 K and P = 2.9 Torr. It can be seen that the measured k'_{1b} values appear to show a more rapid rise in going from $k_{wall}^{(R)}$ at [O_2] = 0 to the slowest k'_{1b} decay with oxygen at [O_2] = 6.7 × 10^{-15} molecule cm^{-3} than in going from this value to the fastest k'_{1b} decay with oxygen at [O_2] = 30 × 10^{-15} molecule cm^{-3}. This first rise may be due to the heterogeneous wall processes. The linear fits were performed to the data sets that includes (solid red line) and excludes (solid blue line) the $k_{wall}^{(R)}$ data-point and fits return the k_{1b} values 2.8 × 10^{-15} cm^3 $molecule^{-1}$ s^{-1} and 2.1 × 10^{-15} cm^3 $molecule^{-1}$ s^{-1}, respectively. Comparing these k_{1b} values give maximum uncertainty 2.8 × 10^{-15} / 2.1 × 10^{-15} = 1.33, which gives ± 33 % uncertainty. In our high-temperature range measurements we often, but not always, observed similar behavior. We take a conservative approach and we estimate our experimental uncertainty to be factor of two, upper limit = 2×k_{1b}, lower limit = 0.5×k_{1b}, in our high-temperature range measurements.

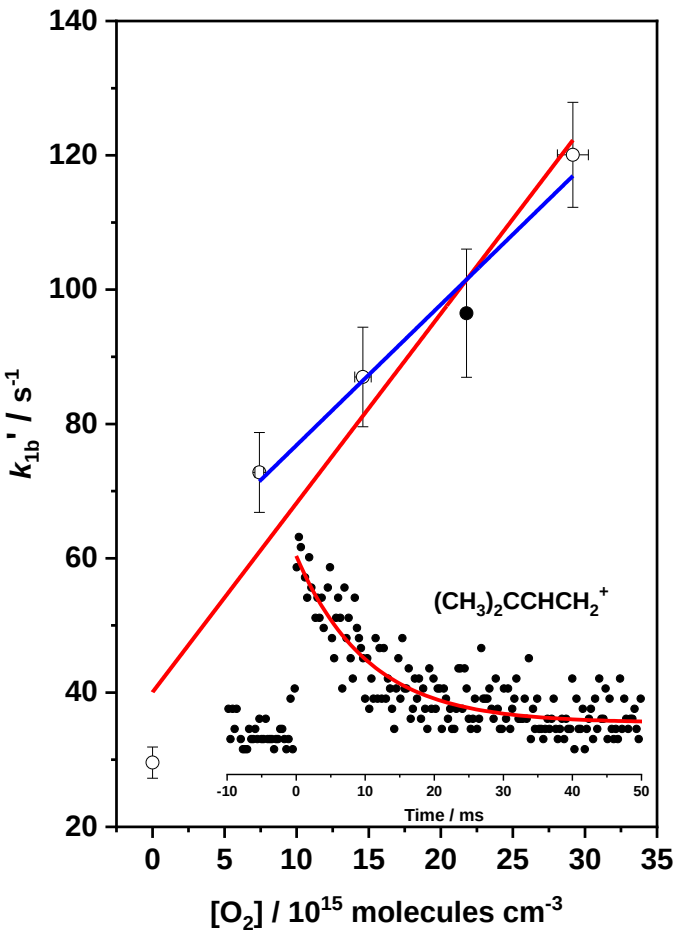

Figure S2. A bimolecular plot of $(CH_3)_2CCHCH_2$ + O_2 → products reaction (1b), measured at T = 501 K and P = 2.9 Torr. The lower right corner of the plot depicts $(CH_3)_2CCHCH_2$ radical decay profile (k'_{1b} = 96.5 ± 9.5 s^{-1}, filled circle in the plot). The uncertainties shown are 1σ. The solid red and blue line depicts the linear fits performed to the data that includes and excludes the $k_{wall}^{(R)}$ data-point, respectively.

Table S2. The MN15/Def2TZVP and CCSD(T)/CBS//MN15/Def2TZVP energies (kcal/mol) of stationary points (relative to reactants R + O_2) for $(CH_3)_2CCHCH_2$ (R) + O_2 reaction, along with their T1 diagnostic values and optimized geometires.

Species	ΔZPE	MN15/Def2TZVP	ROHF-CCSD(T)/CBS	T1	Structure
R + O_2	0	0	0	0.024, 0.017	
P1	1.08	-2.96	-3.08	0.011, 0.032	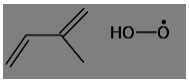
P2	-0.0246	-73.5	-74.2	0.026, 0.013	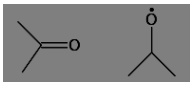
P3	0.905	-22.9	-21.2	0.011, 0.013	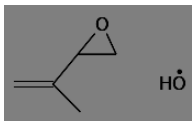
P4	1.05	-40.5	-37.7	0.021, 0.013	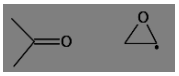
P5	1.78	-40.6	-40.5	0.011, 0.013	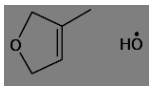
P6	0.312	-34.5	-32.6	0.018, 0.015	
P7	-0.125	-70.0	-69.7	0.021, 0.015	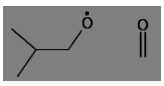

Species	ΔZPE	MN15/Def2TZVP	ROHF-CCSD(T) / CBS	T1	Structure
Int1NT ($ROO_{(nt)}$)	3.79	-21.9	-20.2	0.023	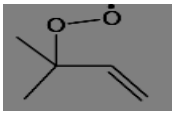

Int1T ($ROO_{(t)}$)	4.28	-20.1	-17.6	0.023	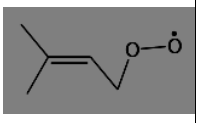
Int2NT	3.14	-7.52	-3.66	0.015	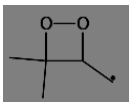
Int2T	3.50	-18.0	-15.3	0.023	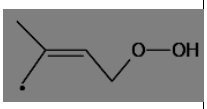
Int3T	3.76	-5.23	0.0200	0.015	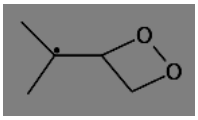
Int4	3.82	-22.2	-18.1	0.014	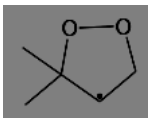
Int5NT	4.28	-49.7	-	-	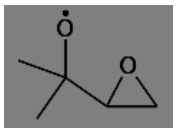
Int5T	3.55	-51.1	-	-	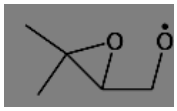

Species	ΔZPE	MN15/Def2TZVP	ROHF-CCSD(T) / CBS	T1
TS1T2TA	0.810	3.32	6.35	0.024
TS1T2TB	0.846	3.35	6.42	0.022

TS1NT2NTA	2.55	7.23	10.1	0.037
TS1NT2NTB	2.49	6.40	-	-
TS1NT4A	2.96	5.22	7.33	0.025
TS1NT4B	2.74	8.97	-	-
TS1NTP1	0.144	4.73	6.11	0.029
TS1T3TA	3.03	6.70	10.4	0.033
TS1T3TB	3.01	8.15	-	-
TS1T4A	3.14	7.76	10.5	0.027
TS1T4B	3.01	9.34	-	-
TS2NT5NT	2.48	12.3	-	-
TS2NTP2A	1.82	9.34	-	-
TS2NTP2B	1.59	5.84	-	-
TS2TP3	1.65	3.17	2.07	0.041
TS2TP5	1.45	12.8	10.9	0.026
TS3T5T	2.83	10.8	-	-
TS3TP7A	1.78	12.1	-	-
TS3TP7B	1.58	14.3	-	-
TS4NT5NT	2.17	10.9	-	-
TS4T5T	2.15	8.61	-	-

Table S3. The results of CASPT2/CBS//MN15/Def2TZVP calculations for the stationary points of $(CH_3)_2CCHCH_2$ (R) + O_2 reaction. Energies in units of kcal/mol.

Species	Active Space	CASPT2/CBS	ROHF-CCSD(T)/CBS (T1 diagnostic)
P1 Channel	13,11		
Int1NT ($ROO_{(nt)}$)		0	0 (0.023)
TS1NTP1		22.8	26.3 (0.029)
P3 Channel	9,9		
Int1T ($ROO_{(t)}$)		0	0 (0.023)
Int2T		-1.22	2.28 (0.024)
TS1T2TA		22.1	23.9 (0.024)
TS1T2TB		22.2	24.0 (0.022)
TS2TP3		12.4	19.6 (0.041)
Non-terminal four-membered ring channel	9,9		
Int1NT ($ROO_{(nt)}$)		0	0 (0.023)
Int2NT		15.4	16.5 (0.015)
ts1NT2NTA		26.7	30.2 (0.037)
ts1NT2NTB		27.6	-
ts2NT5NT		29.4	-
ts2NTP2A		28.2	-
ts2NTP2B		31.2	-
Terminal four-membered ring channel	9,9		
Int1T ($ROO_{(t)}$)		0	0 (0.023)
Int3T		15.9	17.6 (0.015)
TS1T3TA		26.1	27.9 (0.033)
TS1T3TB		25.6	-
TS3T5T		26.9	-
TS3TP7A		31.6	-
TS3TP7B		33.2	-

Five-membered ring channel	7,7		
Int1NT ($ROO_{(nt)}$)		0	0 (0.023)
Int1T ($ROO_{(t)}$)		3.04	2.61 (0.023)
Int4		0.0400	2.09 (0.014)
ts1NT4A		24.9	27.5 (0.025)
ts1NT4B		28.7	-
ts1T4A		28.3	30.7 (0.027)
ts1T4B		29.9	-
ts4NT5NT		27.0	-
ts4T5T		25.5	-